Eur. Phys. J. Plus (2023) 138:96
https://doi.org/10.1140/epjp/s13360-023-03712-z

THE EUROPEAN PHYSICAL JOURNAL PLUS

Regular Article

Numerical simulation and optimization of AC electrothermal microfluidic biosensor for COVID-19 detection through Taguchi method and artificial network

Sameh Kaziz[1,2,a], **Imed Ben Romdhane**[3,b], **Fraj Echouchene**[3,4,c], **Mohamed Hichem Gazzah**[1,d]

[1] Quantum and Statistical Physics Laboratory, Faculty of Sciences of Monastir, University of Monastir, Environment Boulevard, 5019 Monastir, Tunisia
[2] Higher National Engineering School of Tunis, Taha Hussein Montfleury Boulevard, University of Tunis, 1008 Tunis, Tunisia
[3] Laboratory of Electronics and Microelectronics, Faculty of Science of Monastir, University of Monastir, Environment Boulevard, 5019 Monastir, Tunisia
[4] Higher Institute of Applied Sciences and Technology of Soussse, University of Sousse, Sousse, Tunisia

Received: 28 November 2022 / Accepted: 17 January 2023

Abstract Microfluidic biosensors have played an important and challenging role for the rapid detection of the new severe acute respiratory syndrome coronavirus-2 (SARS-CoV-2). Previous studies have shown that the kinetic binding reaction of the target antigen is strongly affected by process parameters. The purpose of this research was to optimize the performance of a microfluidic biosensor using two different approaches: Taguchi optimization and artificial neural network (ANN) optimization. Taguchi L8(2^5) orthogonal array involving eight groups of experiments for five key parameters, which are microchannel shape, biosensor position, applied alternating current voltage, adsorption constant, and average inlet flow velocity, at two levels each, are performed to minimize the detection time of a biosensor excited by an alternating current electrothermal force. Signal to noise ratio (S/N) and analysis of variance were used to reach the optimal levels of process parameters and to demonstrate their percentage contributions, in terms of improved device response time. The principal results of this study showed that the Taguchi method was able to identify that the kinetic adsorption rate is the most influential parameter at 93% contribution, and the reaction surface position is the least influential parameter at 0.07% contribution. Also, the ANN model was able to accurately predict the optimal input values with a very low prediction error. Overall, the major conclusion of this study is both the Taguchi and ANN approaches can be effectively utilized to optimize the performance of a microfluidic biosensor. These advances have the potential to revolutionize the field of biosensing.

Abbreviations

SARS-COV-2	Severe acute respiratory syndrome coronavirus-2
ANN	Artificial neural network
DOE	Design of experiments
ACET	Alternating current electrothermal
S/N	Signal to noise
ANOVA	Analysis of variance
ACE2	Angiotensin-converting enzyme 2
RT-PCR	Reverse transcription polymerase chain reaction
POC	Point-of-care
DF	Degree of freedom
SS	Sum of square
MS	Mean squares

1 Introduction

The severe acute respiratory syndrome coronavirus 2 (SARS-CoV-2) pandemic which was registered in 2019 in Wuhan, China [1], causes the coronavirus disease (COVID-19) responsible for the death of many people in the whole world. Scientific data indicates

[a] e-mail: Kaziz_sameh@yahoo.fr (corresponding author)
[b] e-mail: imbr2110@gmail.com
[c] e-mail: frchouchene@yahoo.fr
[d] e-mail: hichem.gazzah@fsm.rnu.tn

Published online: 29 January 2023

that SARS-CoV-2 is more contagious than the former severe acute respiratory syndrome coronavirus SARS CoV [2] and uses angiotensin-converting enzyme (ACE2), like SARS -CoV, to bind to human cells via its structural S-spike glycoprotein (S protein) [3].

Detection of the SARS-CoV-2 virus has been performed and approved with real-time reverse transcription polymerase chain reaction (RT-PCR) [4]. However, diagnosis by RT-PCR generally requires expensive reagents, specific equipment, and qualified personnel [5]. In addition, the preparation stage is complicated, it takes time, which affects the accuracy of the diagnosis [6]. In order to reduce the detection time of COVID-19 disease, several types of point-of-care (POC) biosensors have been developed [4, 7–9] to detect antigens, antibodies or nucleic acids [10]. Antibody tests are suitable for detecting late-stage infections, while nucleic acid tests detect the presence of nucleic acids (viruses) at an early stage of infection, showing sensitivity and specificity superior to antibody tests. However, nucleic acid testing requires more complicated processes than antibody testing such as nucleic acid extraction, amplification, and detection [11]. Compared to existing POC biosensors, RT-PCR has higher clinical sensitivity and specificity.

Immunoassays, based on the interactions between antigen and antibodies, have attracted tremendous interest in several fields such as medicine and the environment [12, 13]. The detection of SARS-CoV-2 virus can be realized by immunodiagnostic assays by improving specific immunoassays for desired antigen proteins to be reliable and inexpensive. Traditional immunoassays include complex detection protocols and demand skilled professionals. In addition, the inherent diffusion-limited reaction kinetics and the incubation step that sometimes takes hours to reach a detectable level limit their broad applications [14, 15]. Due to unmet medical needs such as early and rapid diagnosis of diseases by detecting very low concentration antigens, immunoassays are increasingly being transferred to microfluidic formats [16]. This emerging miniaturization technology has improved analysis performance by integrating multiple processes into a single chip, so analysis time can be reduced, and sensitivity and reliability can be increased even with low amounts of reagents. Microfluidic chip technology offers the possibility of simultaneously detecting different samples, which are very useful in protein chips. However, the use of microfluidic chips is still limited, due to the limitations of the diffusion transport of antigen in the laminar flow, where lack of target antigen acts as a resistance to its detection and thus for lower antigen concentrations the time required to deliver the antigen to the biosensor becomes longer [14, 15, 17].

In order to improve the sensitivity of microfluidic chips, many numerical and experimental studies have been made [18, 19]. Magnetic effect [20], optical forces [21], electrokinetic effect [22–27], etc., are physical mechanisms that have been applied to agitate the flows in the microchannel to improve the rate of the biosensor binding reaction. Several studies [28, 29] have analyzed the effect of the reaction surface and electrodes shapes for a biosensor excited by an electrothermal force in order to improve the topology of the flow and thus decrease the detection time compared to the same biosensor having a rectangular binding surface. Recently, microfluidic biosensor have been proposed and numerically analyzed and optimized using the finite element method and Taguchi method [30]. Shahbazi et al. [31] showed that the location of the reaction surface relative to the channel inlet has a significant effect on the microfluidic biosensor efficiency. In their study, the authors showed that setting the reaction surface 500 μm from the channel inlet reduced the saturation time by more than 50%.

The detection process in microfluidic biosensors is based on multiple controllable and uncontrollable parameters. The optimal combination of key controllable parameters is essential for the entire process, in terms of device efficiency, decreasing the effects of uncontrollable parameters, as well as reducing process time. Due to the many variables involved in the biosensors detection process, it can be difficult to attribute the individual result to specific parameters. Classical optimization studies involve the variation of one controllable parameter, while the other controllable parameters remain constant. However, these techniques are very painful that can be both expensive and time-consuming [32]. In order to determine the optimal conditions for better manipulation, a time-efficient orthogonal factorial design method known as the Taguchi method was used in this paper because it offers the advantage of optimizing the procedure with less numerical tests required [33]. The Taguchi method is a robust systematic experimental design technique to minimize uncontrollable factors [34] and has been widely used in several fields such as physics [35], medicine [33], environmental science [32, 36], chemical processes [37] and statistics [34]. The Taguchi method is a powerful tool for identifying the optimal combination of design parameters to reduce cost, improve quality and/or increase efficiency. In combination with the Taguchi technique, the analysis of variance (ANOVA) method is a proven method that is used to test the percentage contribution of each parameter on the desired outputs [38]. To optimize a process or a product by the Taguchi approach, three main steps are required, namely system design, parameter design and tolerance design. The design of the system means the clear formulation of the problem to be studied, the definition of the main objectives and the synthesis of knowledge in the fields of application of science and technology. The design of the parameters aims to list the control factors likely to have an influence on the performance of the process under consideration. The optimal condition is chosen such that the effect of noise factors results in minimal variation in system performance.

Tolerance design is a means of refining the results of parameter design by tightening the tolerance of factors that have a significant influence on the product. There are three categories of quality characteristics for signal to noise (S/N) analysis which are the higher-the-better (HB), the lower-the-better (LB), and the nominal-the better. Regardless of the category of the quality characteristic, a higher S/N ratio corresponds to a higher quality characteristic. Therefore, the optimal level of the process parameters corresponds to the one with the highest S/N ratio [39]. Optimizing the biosensor through the design of experiments helps guide efforts to improve the performance of future sensing devices.

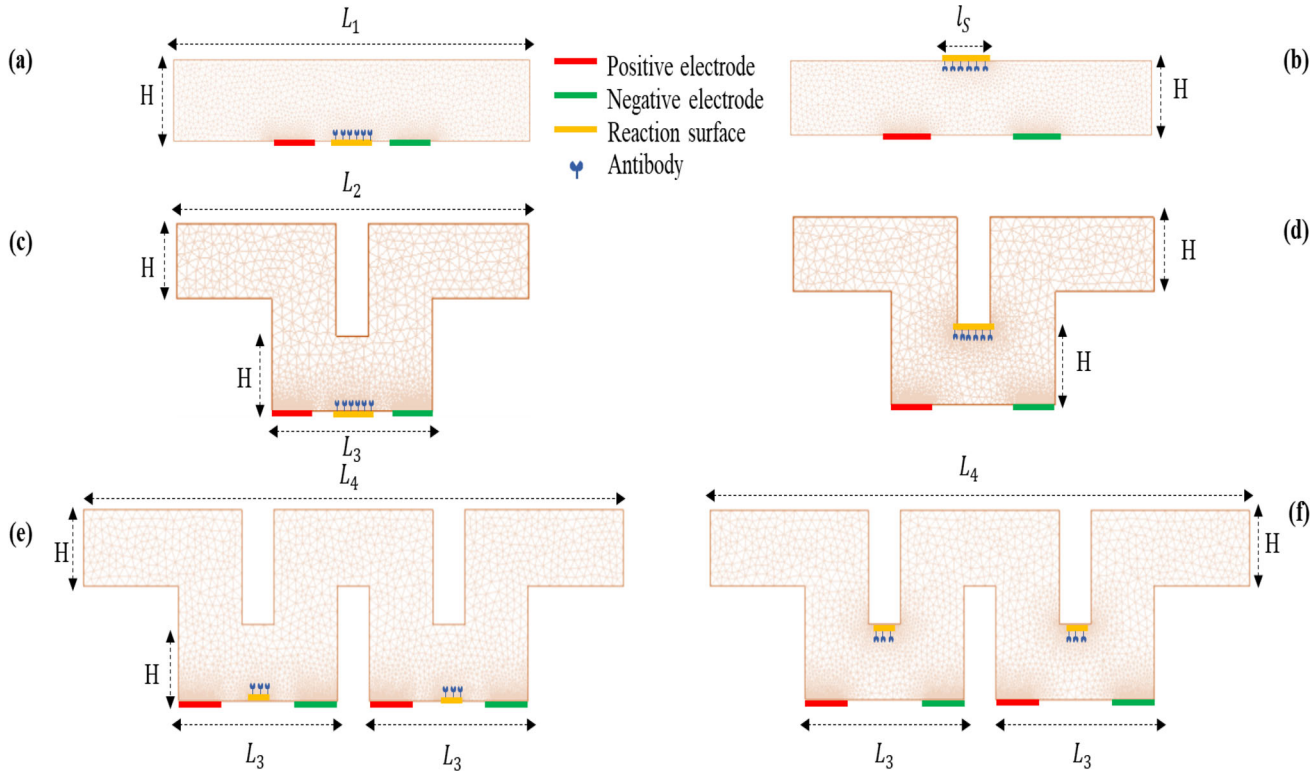

Fig. 1 Design of three types of microfluidic biosensor models. **a** and **b** Straight microfluidic chip; **c** and **d** 1-cycle microfluidic chip; **e** and **f** 2-cycles microfluidic chip

Another area of focus has been on optimizing the use of artificial neural networks (ANNs) in microfluidic biosensors. This has involved exploring different network architectures, training algorithms, and hardware configurations in order to maximize the accuracy and efficiency of the network. The use of ANNs in biosensor optimization is motivated by the ability of these networks to analyze complex data and make predictions based on this analysis, as well as to reduce the need for labor-intensive manual analysis.

In this paper, numerical tests on microfluidic biosensors were first performed to find the optimal combination of design parameters (including microchannel shape, biosensor position, applied AC voltage, adsorption constant, and average flow velocity) using the Taguchi technique, then to examine the contribution of these parameters using the ANOVA method. The global goal is to identify optimal values of key parameters for rapid and efficient detection of SARS-CoV-2. Further, the results of the numerical simulation and the multiple regression model are correlated with the results predicted by the artificial neural network (ANN).

The novelty and significance of the results obtained using the Taguchi method and ANN approach to optimize a biosensor depend on the specific application and the extent to which the optimization improves the performance of the device. In general, any improvement in accuracy or efficiency can be considered significant, as it has the potential to impact a wide range of applications, including rapid disease diagnosis.

2 Numerical procedure

2.1 Geometrical conceptions

Figure 1 illustrates three microfluidic chip designs with different microchannel structures (straight, 1-cycle, and 2-cycles). A pair of electrodes of length $L_E = 10\ \mu$m each was integrated on the lower wall of each microfluidic chip. A reaction surface of length l_S is located at the upper wall, for cases (b), (d) and at the lower wall for cases (a), (c). Two reaction surfaces of length $\frac{l_s}{2}$ each are located at the upper wall, for case (f) and at the lower wall for case (e). All the geometric dimensions for the three types of microfluidic chips are presented in Table 1.

Table 1 Geometrical parameters for the three types of microfluidic chips

Design Parameters	Value
L_1 (μm)	110
H (μm)	20
L_2 (μm)	110
L_3 (μm)	50
L_4 (μm)	190
l_s (μm)	10
L_E (μm)	10

2.2 Electric field calculation

The electric field $\boldsymbol{E}$ was calculated using the Poisson equation (Eq. 1) where V is the electric potential due to the external potential applied across the electrodes.

$$\Delta V = 0 \text{ and } \boldsymbol{E} = -\nabla V \tag{1}$$

2.3 Temperature field calculation

The temperature field in the microchannel fluid was calculated by means of the following thermal energy equation (Eq. 2):

$$\rho C_p \boldsymbol{u} \cdot \nabla T = \lambda \nabla^2 T + \sigma |\boldsymbol{E}|^2 \tag{2}$$

where ρ, λ, σ, C_p and $\boldsymbol{u}$ are the density, the thermal conductivity, the electrical conductivity, the specific heat at constant pressure and the velocity field of the fluid, respectively.

The non-uniform Alternating Current (AC) electric field applied on the fluid induces the variations of the electrical conductivity σ and permittivity ε of the solution due to the temperature gradient generated from the inhomogeneous Joule heating serving as the heat source of the fluid, and it is defined as $\sigma |E|^2$.

Although the electrothermal force applied causes heating of the fluid, the dependence of the specific heat at constant pressure C_p and of the thermal conductivity λ of the fluid as a function of the temperature T can be neglected, since the conduction of the ambient heat allows this received heat to dissipate, thereby the growth of the temperature in the fluid mostly stands low [40]. Here, the viscous dissipation term is smaller than the Joule effect [41], so it has been neglected.

2.4 Flow field calculation

The fluid carrying antigens, supposedly Newtonian and incompressible, flows in a stationary regime inside the microchannel. The Navier–Stokes equations in 2D are thus used to determine the fluid velocity field u in the microchannel as below (Eqs. 3 and 4) where $\langle \boldsymbol{F_e} \rangle$ describes the electrothermal force.

$$\nabla . \boldsymbol{u} = 0 \tag{3}$$

$$\rho (\boldsymbol{u} . \nabla) \boldsymbol{u} = -\nabla p + \mu \nabla^2 \boldsymbol{u} + \langle \boldsymbol{F_e} \rangle \tag{4}$$

Here, p, ρ and μ are the pressure, density, and dynamic viscosity of the fluid, respectively. The applied non-uniform electric field causes non-uniform Joule heating of the fluid inside the microfluidic channel which gives rise to a temperature gradient and therefore to gradients of permittivity and electrical conductivity thus generating the electrothermal force responsible of the agitation of the fluid. The expression of the electrothermal force is given by (Eq. 5):

$$\langle \boldsymbol{F_e} \rangle = -\frac{1}{2} \left(\frac{\nabla \sigma}{\sigma} - \frac{\nabla \epsilon}{\epsilon} \right) \cdot \boldsymbol{E} \frac{\varepsilon \boldsymbol{E}}{1 + (\omega \tau)^2} - \frac{1}{4} \nabla \varepsilon |\boldsymbol{E}|^2 \tag{5}$$

where $\tau = \varepsilon / \sigma$ is the fluid charge relaxation time and ω is the angular frequency of the electric field $\boldsymbol{E}$. The used transporter fluid is water at a temperature close to 293 K, which allowed to consider, according to Green et al. [42], the following equations (Eqs. 6 and 7):

$$\frac{1}{\epsilon} \frac{\partial \epsilon}{\partial T} = -0.004 \Rightarrow \frac{\nabla \epsilon}{\epsilon} = \frac{1}{\epsilon} \frac{\partial e}{\partial T} \nabla T = -0.004 \nabla T \tag{6}$$

$$\frac{1}{\sigma} \frac{\partial \sigma}{\partial T} = 0.02 \Rightarrow \frac{\nabla \sigma}{\sigma} = \frac{1}{\sigma} \frac{\partial \sigma}{\partial T} \nabla T = 0.02 \nabla T \tag{7}$$

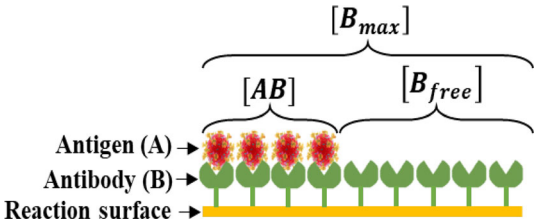

Fig. 2 Antigen–Antibody Kinetic reaction

Therefore, the electrothermal force is given by (Eq. 8):

$$\langle \boldsymbol{F_e} \rangle = -\varepsilon_0 \varepsilon_r \left[0.012(\nabla T \cdot \boldsymbol{E}) \frac{\boldsymbol{E}}{1 + (\omega\tau)^2} - 0.001\left(|\boldsymbol{E}|^2\right)\nabla \mathrm{T} \right] \tag{8}$$

where ε_0 is the permittivity of free space and ε_r is the relative permittivity of the fluid.

2.5 Antigen concentration field calculation

The diffusion-convection transport of target antigen is modeled by the following Fick's second law (Eq. 9):

$$\frac{\partial [A]}{\partial t} + \boldsymbol{u} \cdot \nabla [A] = D \Delta [A] \tag{9}$$

where $[A]$ and D denote the concentration and the diffusion constant of the target antigen, respectively. The binding reaction is confined on the reaction surface ant it is involved only on the boundary condition.

2.6 Reaction kinetics calculation

Antigen molecules (analytes A) are transported by diffusion and convection to free binding sites (ligands B) immobilized on the sensitive surface and an analyte-ligand complex (AB) is formed (Eq. 10):

$$A + B \rightleftharpoons AB \tag{10}$$

According to the first-order Langmuir–Hinshelwood adsorption model [43], the antigen–antibody complex (AB) formation can be described as (Eq. 11):

$$\frac{\partial [AB]}{\partial t} = k_{\mathrm{on}} [A_{\mathrm{surf}}].[B_{\mathrm{free}}] - k_{off} [AB] \tag{11}$$

where $[AB]$; $[A_{\mathrm{surf}}]$; $[B_{\mathrm{free}}]$, k_{on} and k_{off} are the complex surface concentration, the volume analyte concentration (at the binding surface), the surface concentration of free ligands, the complex association kinetic rate and the complex dissociation kinetic rate. The equilibrium of the reaction is described by the equilibrium dissociation constant $K_d = \frac{k_{\mathrm{off}}}{k_{\mathrm{on}}}$. As explained in Fig. 2, the concentration of available binding sites on the sensitive surface, $[B_{max}]$, is equal to the sum of the concentrations of free binding sites, $\left[B_{free}\right]$, and that of bound complexes $[AB]$ (Eq. 12):

$$[B_{\mathrm{max}}] = [B_{\mathrm{free}}] + [AB] \tag{12}$$

The Eq. (11) is then written as (Eq. 13):

$$\frac{\partial [AB]}{\partial t} = k_{\mathrm{on}} [A_{\mathrm{surf}}].([B_{\mathrm{max}} - [AB]]) - k_{\mathrm{off}} [AB] \tag{13}$$

3 Boundary and initial conditions

An electric potential of $\pm V_{rms}$ and a temperature T_0 equal to that of the ambient have been applied to the electrodes. The walls, reaction surface, inlet, and outlet are assumed to be electrically insulated. In the matter of the thermal boundary conditions, the walls and reaction surface are presumed to be thermally insulated. Heat flow is exchanged at the inlet and outlet of the channel. For the modeling of the laminar flow, at the inlet of the microfluidic channel the fluid flows with a parabolic velocity profile of average value U_{ave} and, at the outlet the flow is supposed to be completely developed. For the lower and upper microchannel walls including the reaction surface, the no-slip condition was applied. Concerning the modeling of antigen transport, a constant volume concentration $[A]_0$ and a convective flow condition, $\overrightarrow{n}.(D\nabla[A]) = 0$, were imposed, respectively at the inlet and at the outlet of the microchannel. for the reaction surface, the condition of diffusive flux balanced by the temporal flow rate was applied and for the rest of the microchannel walls, it is assumed to be impermeable (do not interact with the target antigens) and the homogeneous Neumann condition was adopted [31]. For the initial conditions concerning Eqs. (12) and (13), the analyte and surface complex concentrations were initially set to zero: $[\boldsymbol{A}]_{(t=0)} = 0$ and $[\boldsymbol{AB}]_{(t=0)} = 0$.

Table 2 Model parameters

Constant	Name	Value
λ(W/(K·m))	Thermal conductivity	0.6
ρ(kg/m^3)	Fluid density	1000
μ(Pa.s)	Dynamic viscosity	1.08×10^{-3}
Cp(kJ/(kg·K))	Specific heat capacity	4.184
σ(S/m)	Electrical conductivity	5.75×10^{-2}
ε_r	Relative permittivity	80.2
f(kHz)	Frequency	100
D(m^2/s)	Diffusion coefficient	10^{-11}
[$\mathbf{B_{max}}$]mol/m^2	Surface ligand concentration	3.3×10^{-8}
[A_0]mol/m^3	Analyte input concentration	10^{-9}

4 Numerical simulations

In order to solve the model equations, the finite element method was adopted [44]. The 2D domain has been discretized into triangular cells and refined near the sensitive surface. First the electric field has been calculated by means of the electrostatic equation, then the fields of temperature and velocity are obtained by solving together the steady-state Navier–Stokes and thermal energy equations. Finally, the concentration of the target antigen, $[A](x, y, t)$ in the microchannel and the concentration of the antigen–antibody complex, $[AB](x, t)$ on the sensitive surface were obtained by simultaneously solving the antigen transport and the binding reaction equations in a time-dependent regime. Here, the target antigen is the SARS-CoV-2 virus, and the ligand is its antibody (b1 or h12) [31, 45].

The detection time of the microfluidic biosensor constitutes the main parameter of the analyte-ligand chemical kinetics, and it corresponds to the time during which the concentration of the analyte-ligand complex reaches 95% of its threshold value. To obtain the total concentration of the formed complexes (SARS-CoV-2-antibody), the local concentration was integrated over the entire length of the binding surface (Eq. 14) and the normalized surface concentration of these complexes, $[\overline{AB}]$, was calculated by dividing the total concentration by the concentration of binding sites on the surface of the biosensor, $[B_{\max}]$.

$$\langle [\boldsymbol{AB}] \rangle = \frac{1}{\boldsymbol{l_s}} \int_0^{\boldsymbol{l_s}} [\boldsymbol{AB}](x, t) \mathrm{d}x \tag{14}$$

where $\boldsymbol{l_s}$ is the length of the binding surface.

All the physical and biological (binding) parameters of SARS-CoV-2 S protein/Antibody [24, 31] used for this numerical study are illustrated in Table 2. In cases of 2-cycles microfluidic chips, the concentration of binding sites on the reaction surface is $[B_{\max}]/2$.

5 Results and discussions

5.1 Model validation

First, the numerical model was tested by comparison with experimental existing data of Berthier and Silberzan [31], as shown in Fig. 3. The time-normalized surface concentration during the adsorption phase was calculated using the same experimental parameters using a microfluidic channel with 1 mm high and 1 cm wide. The concentration of the target antigens and their diffusion constant are respectively 2.5×10^{-6} Mol/m^3 and 7×10^{-11}m^2/s. The flow rate of the carrier fluid is 10^{-6} m^3/s. The density of binding sites, association and dissociation constant are 1.668×10^{-8} Mol/m^2, 75 m^3/Mol.s and 10^{-2} s^{-1}, respectively. We can note that the average error between the two results is very small which makes it possible to consider that the model is proven, and that it can be used for other topics.

5.2 Binding enhancement by electrothermal force

ACET agitation flow can be used to accelerate the transport of antigen in suspension to the reaction surface, providing more opportunities for binding between antigens and antibodies. The normalized concentrations of the antigen/antibody complexes predicted by the numerical model during the association phase, without and with an applied electric field (10 V) and when the reaction surfaces are placed on the lower or the upper walls are shown in the Fig. 4.

As shown in Fig. 4, the antigen–antibody binding efficiency increases with the electrothermal effect, especially for the 2-cycles structure regardless of the position of the reaction surface.

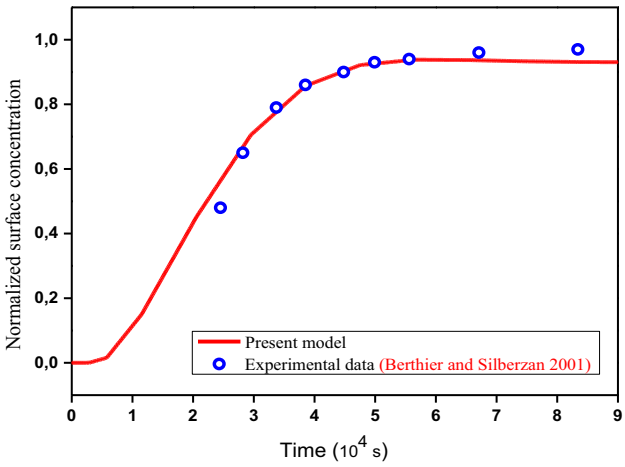

Fig. 3 Comparison of present model with the experimental results of Berthier and Silberzan [26]

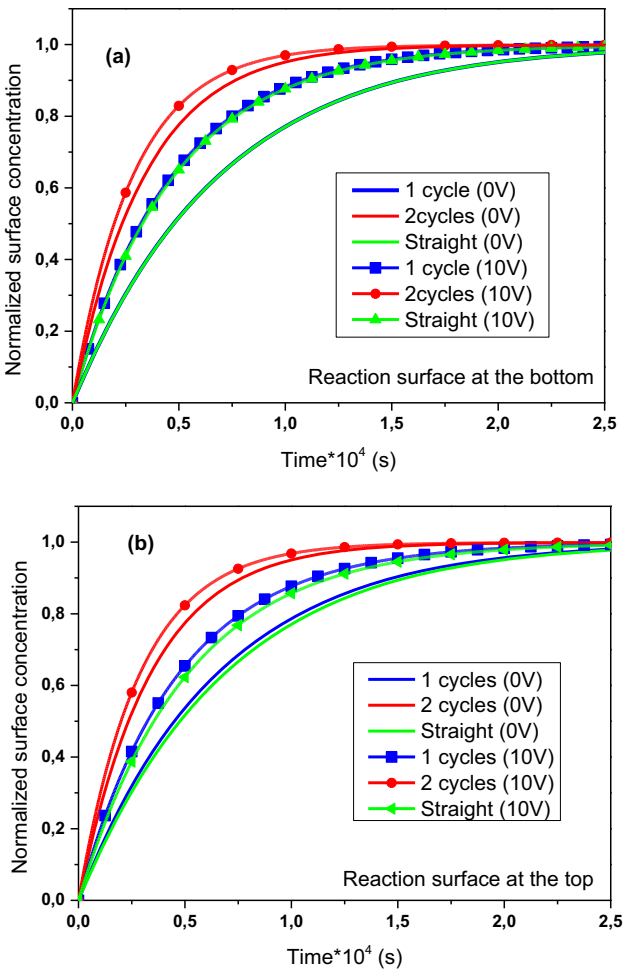

Fig. 4 Normalized surface concentration during the adsorption phase for the three microfluidic chips without and with electrothermal effect. **a** The reaction surfaces are on the bottom and **b** The reaction surfaces are on the top

5.3 Experimental design

The Taguchi method for the “design of experiments” (DOE) was considered in this numerical simulation in order to reduce the list of tests to be performed to obtain the lowest detection time of the microfluidic biosensor. Table 3 shows the five factors acting on the detection system, each taking two levels. If there are five factors called A, B, C, D and E, all of them are examined with two levels called "-1" and "1", which represent the lowest and highest levels, respectively, then according to the complete plan, the number of experiments to be carried out should be $2^5 = 32$ trials. To reduce this number, the orthogonal table L8(2^5), based on Taguchi’s

Table 3 Selected optimization factors and respective levels

Symbol	Optimization Factor (Unit)	Low level (-1)	High level (1)
A	Microchannel type	1-cycle	2-cycles
B	Biosensor position	Bottom	Top
C	Applied voltage, V_{rms}(V)	0	10
D	Adsorption constant, k_{on} (m^3/ (Mol.s))	100	10,000
E	Average inlet velocity, U_{ave}(m/s)	0.0001	0.0005

Table 4 The Taguchi $L_8\left(2^5\right)$ orthogonal table

Experiment run	Factors levels				
	A	B	C	D	E
1	− 1	− 1	− 1	− 1	− 1
2	− 1	− 1	− 1	1	1
3	− 1	1	1	− 1	− 1
4	− 1	1	1	1	1
5	1	− 1	1	− 1	1
6	1	− 1	1	1	− 1
7	1	1	− 1	− 1	1
8	1	1	− 1	1	− 1

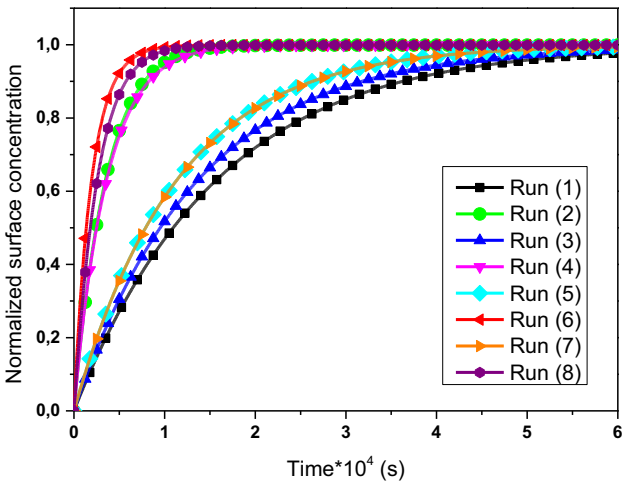

Fig. 5 Normalized complex concentration versus time for the nine Taguchi tests

method, was used, and was presented in Table 4. This plan requires only eight experiments with five critical parameters at two levels each, while neglecting the interactions between them.

For each test, the factors are defined at levels − 1 or 1. Figure 5 illustrate the average normalized antigen–antibody complex concentration versus time for all experiment tests of Table 4.

For Taguchi design of experiments, we can manipulate the noise factors to force the variability and fix, from the obtained results, the optimal parameters that make the detection process robust or resistant to the variation due to these noise factors. When the values of a signal-to-noise ratio (S/N) are high, it means that the control factor parameters limit the effects of the noise factors. The values of S/N ratio for the three experimental objectives which are the nominal is the best, smaller is the best and the lager is the best, are resumed on Table 5. S is the signal value, N is the noise value, n is the number of simulation test and y_i is the measured response value (response of the simulation ith). A high value of S/N indicates a good performance [39] and the optimal level of each parameter is then specified by a greater S/N values.

In our case, the S/N ratio values were calculated based on "smaller is better" criteria for each test because we aimed to minimize the detection time of the device. Table 6 shows the numerical results for the response time of the biosensor T_R, the corresponding S/N ratios and the fluid tempertaures rise (ΔT) using the experimental layout.

The increase in the temperature of the fluid for the eight simulations did not exceed the limit value (5°K) [41, 46], which proves the good choice of the applied voltage levels.

To assess the effect of each key parameter, the mean values of the responses obtained for each level must be calculated. To do this, the sum of the results associated with each level of the orthogonal table divided by the number of tests for this level provides the

Table 5 S/N ratio experimental aims and equations

S/N ratio	Experimental objective	S/N Ratio expression
Nominal is the best	Negative, zero or positive	$S/N = -10\log\left(\frac{1}{n}\sum_{i=1}^{n}\left(y_i^2 - y_0^2\right)\right)$
Smaller is the best	Minimize the response	$S/N = -10\log\left(\frac{1}{n}\sum_{i=1}^{n} y_i^2\right)$
Larger is the best	Maximize the response	$S/N = -10\log\left(\frac{1}{n}\sum_{i=1}^{n}\frac{1}{y_i^2}\right)$

Table 6 Taguchi orthogonal array results for the biosensor detection time T_R and the respective calculated S/N values

Run	Factor						Results	
	Type-mic	Position	V_{rms}(V)	k_{on}	U_{ave}	T_R(min)	S/N ratio	ΔT(°K)
1	1-cycle	Down	0	100	0.1	786.25	− 57.91	0.00
2	1-cycle	Down	0	10,000	0.5	164.58	− 44.33	0.00
3	1-cycle	Up	10	100	0.1	690.41	− 56.78	4.77
4	1-cycle	Up	10	10,000	0.5	177.91	− 45.00	4.77
5	2-cycles	Down	10	10	0.5	570.83	− 55.13	4.82
6	**2-cycles**	**Down**	**10**	**10,000**	**0.1**	**97.91**	**− 39.82**	**4.80**
7	2-cycles	Up	0	100	0.5	571.25	− 55.14	0.00
8	2-cycles	Up	0	10,000	0.1	122.91	− 41.79	0.00

The meaning of the bold is to distinguish the optimal test found

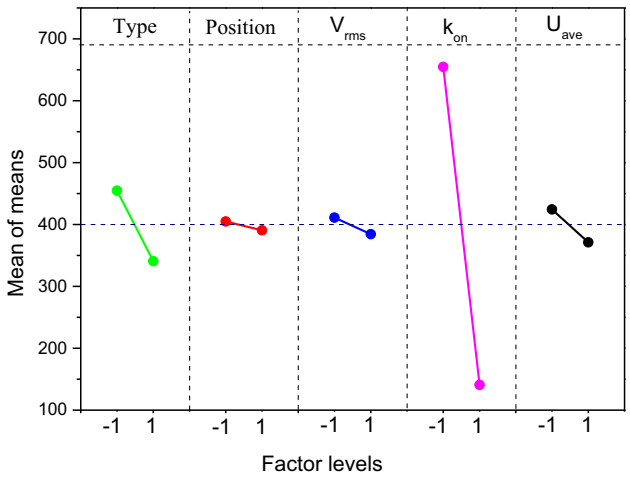

Fig. 6 Main effect plots of each key parameter on the detection time of the device

appropriate averages. Figure 6 shows the average effect of the four factors used in this study. The factor with the strongest influence was determined by the difference values, Delta, between the maximum value and the minimum value of average values obtained. The greater the difference, the more influential the control factor. From the Fig. 6 of responses, it is evident that the adsorption constant rate has the strongest influence.

The importance of each key parameter can be determined as shown in Table 7, by subtracting the maximum S/N ratio from its minimum value across the two levels. The parameter that has the least difference in the S/N ratio has less role in controlling the synthesis process [47]. By plotting the S/N ratio against each of the key parameters according to the values of Table 7, it is easily seen in Fig. 7 that, according to the Taguchi method, the lowest value of the response time of the biochip is reached with 2-cycles microfluidic channel having a reaction surface on the bottom at the highest levels of the applied voltage (10 V) and the adsorption rate (10^4) and lowest level of the average flow velocity (0.1 mm/s). The optimal combination ($A_1B_{-1}C_1D_1E_{-1}$) was among the eight runs of the L8 orthogonal network (test6), that Taguchi's method was able to detect it.

5.4 ANOVA analysis: percentage contribution of the controllable parameters

Following the ANOVA scheme used for the L8 Taguchi method [48], the percentage contribution of each key parameter on the detection time are determined in this work. The equations used in this analysis are as follows (Eqs. 15–19):

Table 7 Signal to Noise Ratios for each level

Level	Type	Position	V_{rms}	k_{on}	U_{ave}
− 1	− 51.01	− 49.30	− 49.79	− 56.24	− 49.08
1	− 47.97	− 49.68	− 49.18	− 42.73	− 49.90
Δ = Max − Min	**3.04**	**0.38**	**0.61**	**13.51**	**0.82**
Rank	2	5	4	1	3

The meaning of the bold is to show that the difference (Δ = Max − Min) in the S/N ratios allows determining the effects of the design parameters in the detection process. Whoever has the least difference has less effect and vice versa

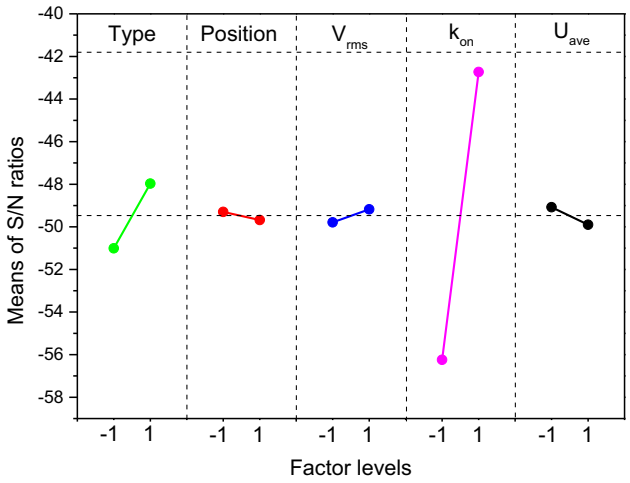

Fig. 7 S/N ratio for the five key parameters at different levels

- The average of all response times $\overline{T}_R$ in the Taguchi design is:

$$\overline{T}_R = \frac{1}{8}\sum_{i=1}^{8} T_{R_i} \tag{15}$$

- The total sum of squares SS_{Total} is:

$$SS_{\text{Total}} = \sum_{i=1}^{8} \left(T_{Ri} - \overline{T}_R\right)^2 \tag{16}$$

- The sum of squares for microfluidic structure, biosensor position, applied voltage, adsorption constant and average inlet velocity are respectively:

$$SS_i = 2\sum_{i=1}^{2} \left(T_{Rxi} - \overline{T}_R\right)^2 \tag{17}$$

where $T_{R_{xi}}$ is the i-th average response time of the corresponding parameter x (Type, Position, Voltage, k_{on} and average inlet velocity) in the Taguchi design.

- The mean squares (MS) for each parameter i are expressed with:

$$MS_i = \frac{SS_i}{DF_i} \tag{18}$$

where DF is the degree of freedom (1 = number of level– 1).

- *The contribution percentages* for each parameter i are then:

$$\%\text{Contribution}_i = \frac{SS_i}{SS_{\text{Total}}} \tag{19}$$

The obtained results are presented in Table 8 and Fig. 8. Among the selected key parameters, the adsorption constant (k_{on}) has the highest contribution (93%) to the reduction of the response time of the device, while the position of the reaction surface has the lowest contribution (0.07%). These results are in agreement with the results of Shahbazi et al. [31] who showed that the saturation time would increase by 40% when the adsorption and dissociation rates are reduced by a factor of 10. The adsorption rates are very influential than the other parameters.

Table 8 ANOVA results on the detection time response

Source	DF	SS	MS	% Contribution
Type	1	26,021	26,021	4.6
Position	1	407	407	0.072
V_{rms}	1	1456	1456	0.26
k_{on}	1	528,099	528,099	**93.5**
U_{ave}	1	5666	5666	1
Residual Error	2	3131	1565	0.55
Total	7	564,780	–	100

The significance of bold is to show the highest contribution (93%) of the most influential parameter in reducing the response time of the device

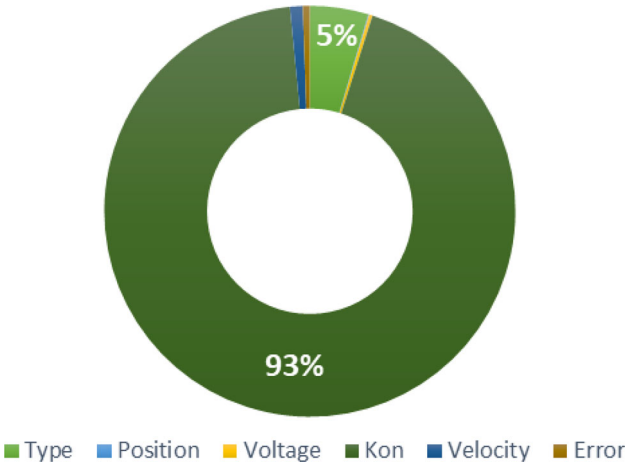

Fig. 8 Contributions of key parameters on biosensor detection time

5.5 Checking the optimum values

Under the optimal setting conditions, the optimal value of the microfluidic biosensor response time is estimated as follows:

$$\widehat{T}_R = \overline{T}_{\text{Type}_1} + \overline{T}_{k_{\text{on}}1} - \overline{T}_R = 340.73 + 140.83 - 397.76 = 83.8\text{min} \tag{20}$$

where $\overline{T}_{Type_1}$ is the average response time for $Type$ parameter at high level (level 1) obtained from Table 6, $\overline{T}_{k_{on}1}$ is the average response time for k_{on} parameter at high level (level 1) obtained from Table 6 and $\overline{T}_R$ is the mean of all response times. By running the FEM simulation under the optimal tuning conditions, we can get $T_R = 97.91$min, then the relative error: $\left|\frac{T_R - \widehat{T}_R}{T_R}\right| \times 100 = 14.4\%$ which is accebtable, knowing that we have taken into account only the two most influential variables.

Figure 9 shows the antigen diffusion boundaries layers just near the reaction surface at the adsorption times (1000 s) for test 3, test 4, test 5 and test 6 where the electrothermal effect was present. The diffusion boundary layer thickness at the test 6 is very thin, which shows that the mass transport is sufficient for the analyte-ligand bond for the optimal test, which has led to an improvement in the efficiency of the biosensor. Moreover, Fig. 10 which shows the velocity field and the flux lines for the four tests having the ACET effect affirms that the fluid is more agitated in the optimal test 6.

5.6 Multiple regression analysis

Multiple regression is used to predict the relationship between variables. Multiple linear regressions take the following expression:

$$Y = a_0 + \sum_{i=1}^{N} a_i x_i \tag{21}$$

where $Y \equiv T_R$ is the response, a_0 is the average of response, x_i are the known variables ($x_1 \equiv Type$, $x_2 \equiv$ Position, $x_3 \equiv V_{\text{rms}}$, $x_4 \equiv k_{\text{on}}$, $x_5 \equiv U_{\text{ave}}$) on which predictions are to be made and a_i are the coefficients which are calculated by the least squares method using the Matlab software:

$$\boldsymbol{T_R} = 397.8 - 57\boldsymbol{x}_1 - 7.1\boldsymbol{x}_2 - 13.5\boldsymbol{x}_3 - 256.9\boldsymbol{x}_4 - 26.6\boldsymbol{x}_5 \tag{22}$$

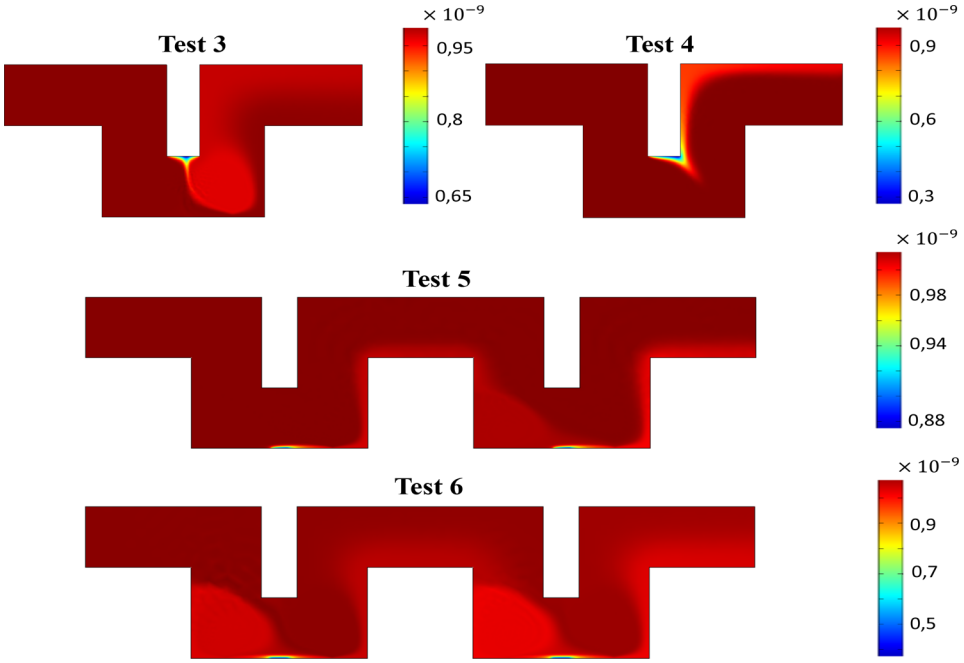

Fig. 9 Analyte concentration diffusion boundary layers in adsorption phase for electrothermal effect tests

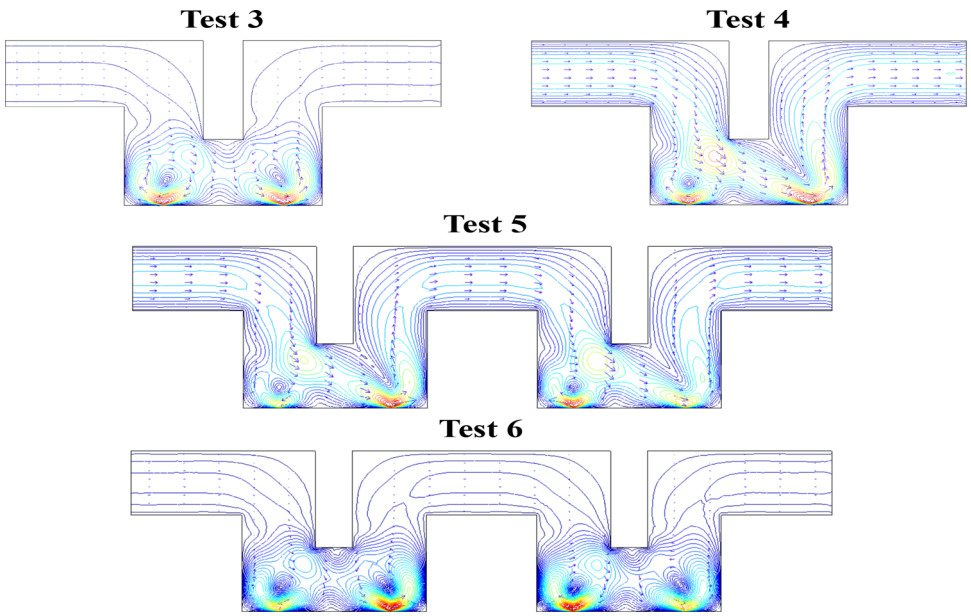

Fig. 10 Velocity field and flow lines for the four tests having the ACET effect

The detection time T_R of the microfluidic biosensor is calculated by Eq. (22). In multiple regression analysis, the regression coefficient (R^2) is 0.98 indicating that about 98% of the variability in the data has been explained by this model (Eq. 22).

Figure 11 illustrates the direct effects of all the control variables (x_1, x_2, x_3, x_4 and x_5) on the microfluidic biosensor response time. These results come from the multiple regression model. The T_R isolines as a function of the control variables presented in Fig. 11 show the direct effect of all the control parameters on the response time of the detection device.

5.7 Artificial neural network

For physical problems with several variables, their dependent models are too complicated. For the case of our problem, the response time of the microfluidic biosensor depends on several variables. We want to find a simple model to model it. For this, artificial neural networks (ANN) show their effectiveness for this type of problem. An artificial neuron is a very simple mathematical operator having inputs which can be the outputs of other neurons, or external signal inputs, and an output. In this section, a multilayer

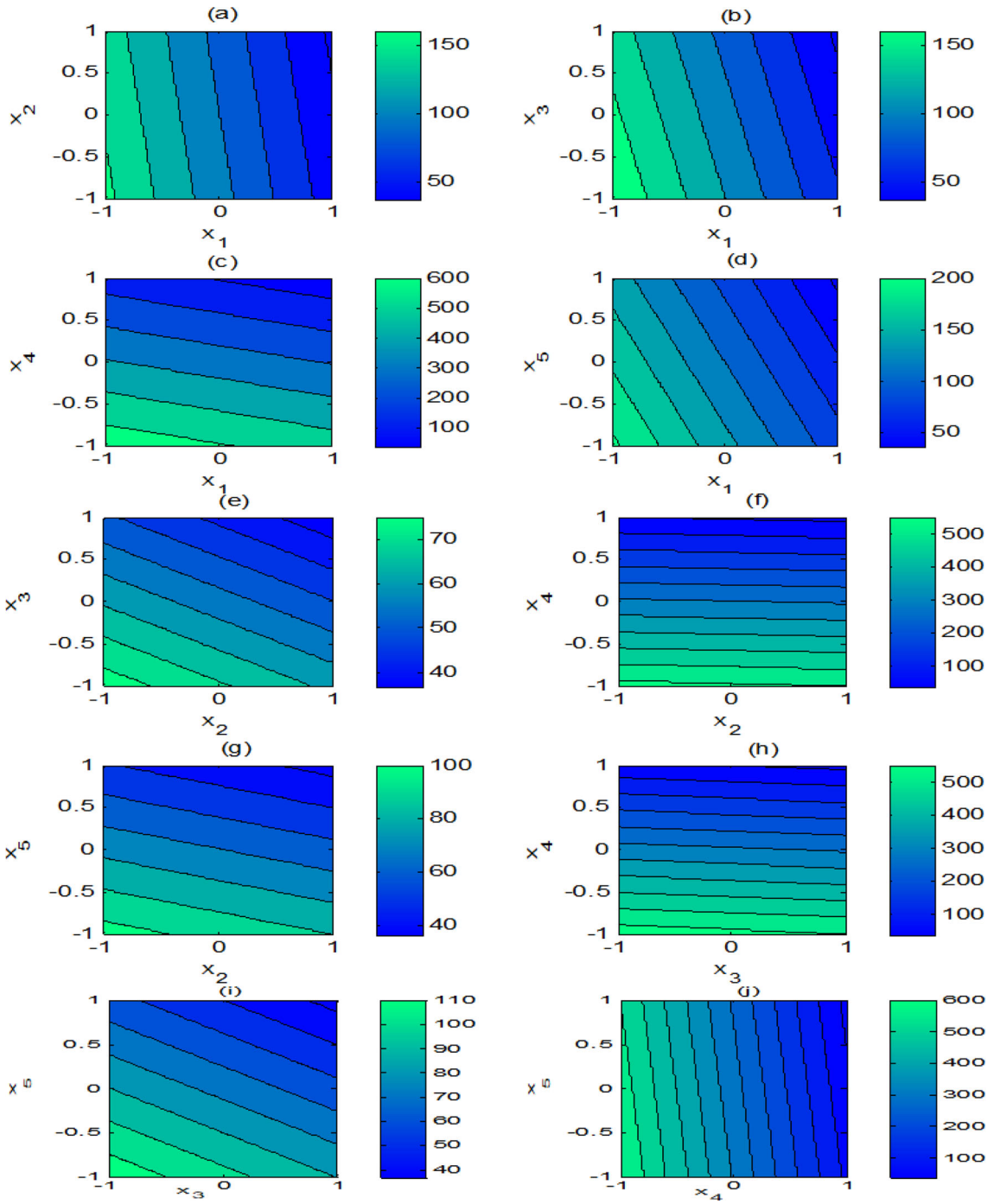

Fig. 11 **a–j** Effects of control parameters on response time T_R

backpropagation neural network was adopted in the microfluidic biosensor to predict its performance in terms of detection time. Artificial Neural Network (ANN) modeling is done through two processes:

- Network formation;
- Analyze the network according to the input data.

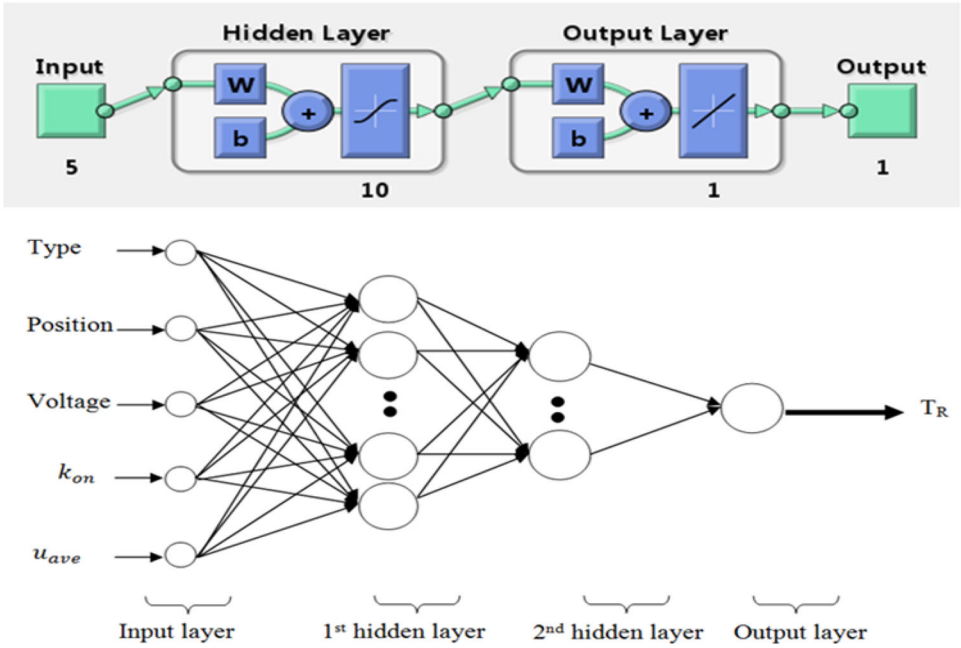

Fig. 12 Block diagram of artificial neural network

The scaled conjugated gradient algorithm, based on the error correction learning rule, is used to solve complex problems.

The network is validated using all simulation factors (type, position, V_{rms}, k_{on}, U_{ave}) as input to the network and the predicted output (detection time) is correlated with the actual values. If the discrepancy between the predicted values and the simulation values is large, the network is recycled by varying the number of neurons and hidden layers. In this study, 10 neurons in the hidden layers are used (Fig. 11) and the calculations are performed using the neural network fitting (nft) toolkit available in MATLAB R-2010a.

After processing its input through the activation function, each neuron produces its output. In this ANN model, the hyperbolic tangent function has been adopted. There are mainly two ways to improve the performance of the neural network: add more training cases or reduce the number of input factors. In our case, the input data as well as the outputs presented in the Taguchi table are small (8 inputs for each variable and 8 outputs). For this, we increased the number of data points using a full factorial design (2^5) based on ANOVA analysis to improve network performance. The regression between network outputs and corresponding targets during the training, validation, testing and all data sets processes is shown in Fig. 12. The best match is very close to the ideal model (shown in the dotted line). An efficient neural network is one that regresses during these various processes with an R value very close to unity.

The high values of R (approximately unity) indicates that the ANN model is very effective in predicting microfluidic biosensor responses.

Figure 13 presents a comparison of the results of the biosensor detection time calculations found by simulation, ANN and multiple regression model. The obtained results showed that regression and ANN are effective optimization tools and that ANN was slightly better than the regression model (Fig. 14).

The design and optimization of an efficient, inexpensive, and reliable microfluidic biosensor in a short time aimed at combating pandemics may be possible via numerical simulation. On the other hand, the use of a simpler mathematical model for detection system optimization is possible via multiple regression. In addition, the use of artificial intelligence for complex cases is important. This new architecture is designed for microfluidic biosensors since it reduces the amount of reagent, energy consumption, and costs. These results prove the usefulness of numerical simulation and especially the use of artificial intelligence, which makes it possible to model complex systems with several control factors. On the other hand, the use of the Taguchi method combined with the analysis of variance (ANOVA) shows its effectiveness in reducing the number of experiments and in determining the significance of the control factors. In comparison with the literature presented in the introduction, this new optimization method seems the best since it combines the minimization of the number of tests for simulation as well as artificial intelligence.

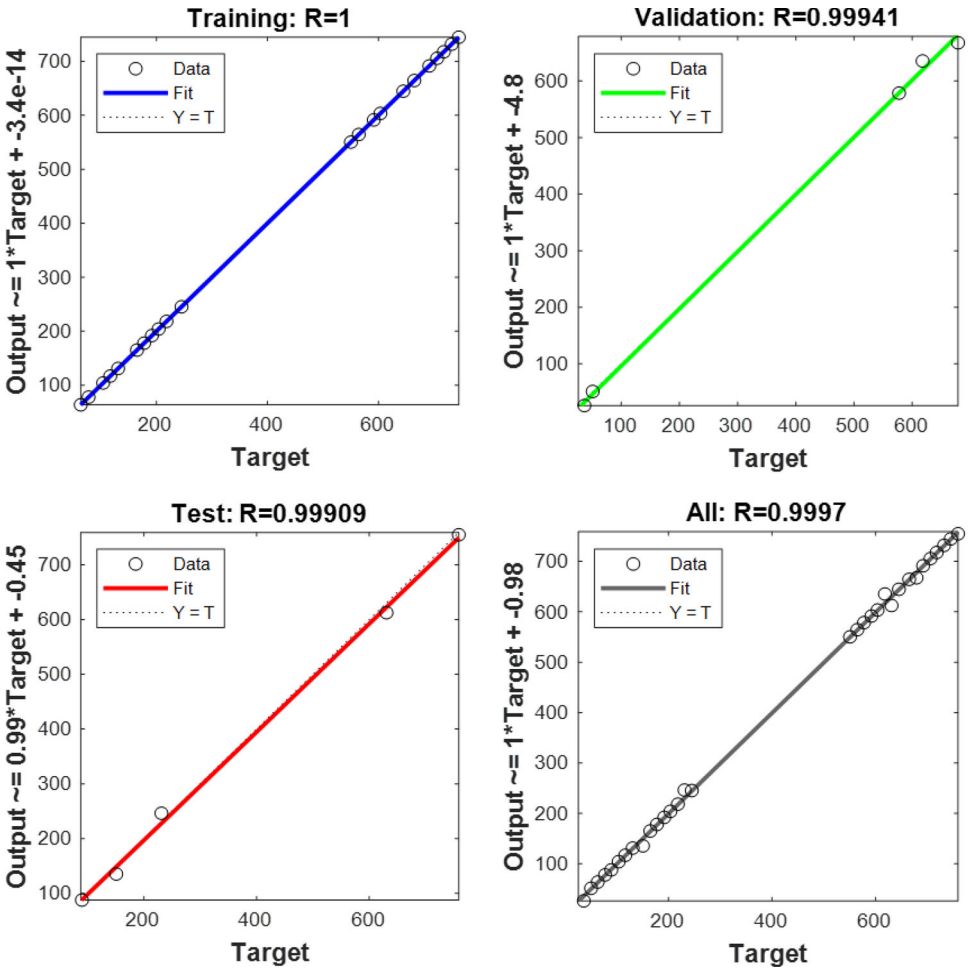

Fig. 13 Regression of estimated values versus numerical values for the ANN model

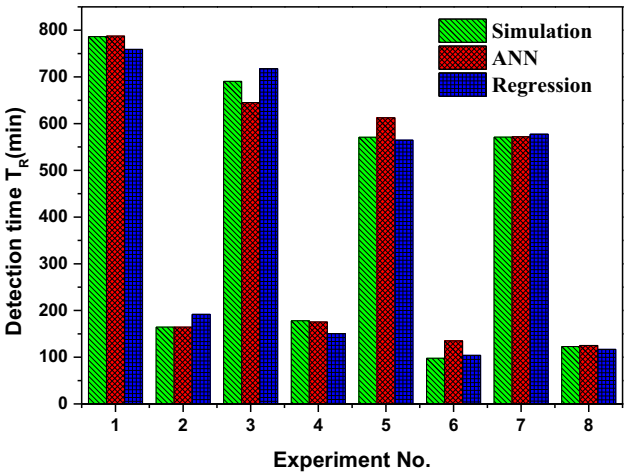

Fig. 14 Comparison of the estimated values of detection time obtained with the regression and ANN models against the simulation values

6 Conclusion

This work aims to numerically optimize a microfluidic chip excited with electrothermal force for rapid bioassays for COVID-19 disease. We analyzed the kinetics of the SARS-CoV-2 binding reaction according to some control parameters namely the microfluidic

chip structure, the position of the reaction surface, the applied voltage, the adsorption rate, and the input fluid velocity. The analysis shows that the DOE's approach based on Taguchi method is appropriate to solve this numerical problem. Instead of using full factor analysis requiring a total of 32 runs of simulations, the L_8 orthogonal array consisting of five factors of two levels each and a total of only 8 runs was used. The results showed that the optimal combination of key parameters tested for the current study is $\text{Type}_1\text{Position}_{-1}V_{rms\,1}k_{on\,1}U_{ave-1}$ for the best device answer. Therefore, the optimal combination of high-performance biosensor enhanced with electrothermal effect and intended for SARS-CoV-2 detection mainly depends on the 2-cycles microfluidic structure, reaction surface on the bottom wall of the microchannel, applied voltage at level 1 (10 V), adsorption constant at level 1 (10,000) and average inlet velocity at level − 1 (0,1 mm/s), which reduced the detection time to **97.91** min. The regression model and artificial neural network (ANN) developed can predict the response time. These advances have the potential to revolutionize the field of biosensing, enabling the rapid and accurate analysis of a wide range of biological samples in a variety of applications.

Data availability The data included in this manuscript are available and can be discussed (or shared), upon request to the corresponding author Sameh Kaziz.

References

1. M. Fani, A. Teimoori, S. Ghafari, Comparison of the COVID-2019 (SARS-CoV-2) pathogenesis with SARS-CoV and MERS-CoV infections. Futur. Virol. **15**(5), 317–323 (2020)
2. M.A. Shereen, S. Khan, A. Kazmi, N. Bashir, R. Siddique, COVID-19 infection: emergence, transmission, and characteristics of human coronaviruses. J. Adv. Res. **24**, 91–98 (2020)
3. Y. Huang, C. Yang, X.-F. Xu, W. Xu, S.-W. Liu, Structural and functional properties of SARS-CoV-2 spike protein: potential antivirus drug development for COVID-19. Acta Pharmacol. Sin. **41**(9), 1141–1149 (2020)
4. J.R. Choi, Development of point-of-care biosensors for COVID-19. Front. Chem. **8**, 517 (2020)
5. S.V. Vemula, J. Zhao, J. Liu, X. Wang, S. Biswas, I. Hewlett, Current approaches for diagnosis of influenza virus infections in humans. Viruses **8**(4), 96 (2016)
6. C.T. Pachucki, M.A. Khurshid, J. Nawrocki, Utility of reverse transcriptase PCR for rapid diagnosis of influenza a virus infection and detection of amantadine-resistant influenza a virus isolates. J. Clin. Microbiol. **42**(6), 2796–2798 (2004)
7. J.R. Choi, A. Nilghaz, L. Chen, K.C. Chou, X. Lu, Modification of thread-based microfluidic device with polysiloxanes for the development of a sensitive and selective immunoassay. Sens. Actuator B Chem. **260**, 1043–1051 (2018)
8. X. Kou et al., Smartphone-assisted robust enzymes@ MOFs-based paper biosensor for point-of-care detection. Biosens. Bioelectron. **156**, 112095 (2020)
9. O. Pashchenko, T. Shelby, T. Banerjee, S. Santra, A comparison of optical, electrochemical, magnetic, and colorimetric point-of-care biosensors for infectious disease diagnosis. ACS Infect. Dis. **4**(8), 1162–1178 (2018)
10. J. Zhifeng, A. Feng, T. Li, Consistency analysis of COVID-19 nucleic acid tests and the changes of lung CT. J. Clin. Virol. **127**, 104359 (2020)
11. R. Tang et al., A fully disposable and integrated paper-based device for nucleic acid extraction, amplification and detection. Lab Chip **17**(7), 1270–1279 (2017)
12. M. Fani et al., Current approaches for detection of human T-lymphotropic virus type 1: a systematic review. J. Cell. Physiol. **234**(8), 12433–12441 (2019)
13. M. Sigurdson, D. Wang, C.D. Meinhart, Electrothermal stirring for heterogeneous immunoassays. Lab Chip **5**(12), 1366–1373 (2005)
14. D.B. Hibbert, J.J. Gooding, P. Erokhin, Kinetics of irreversible adsorption with diffusion: application to biomolecule immobilization. Langmuir **18**(5), 1770–1776 (2002)
15. K.-R. Huang et al., Simulation on binding efficiency of immunoassay for a biosensor with applying electrothermal effect. J. Appl. Phys. **104**(6), 064702 (2008)
16. E.K. Sackmann, A.L. Fulton, D.J. Beebe, The present and future role of microfluidics in biomedical research. Nature **507**(7491), 181–189 (2014)
17. N.S. Lynn Jr. et al., Biosensing enhancement using passive mixing structures for microarray-based sensors. Biosens. Bioelectron. **54**, 506–514 (2014)
18. M. Selmi, F. Echouchene, H. Belmabrouk, Analysis of microfluidic biosensor efficiency using a cylindrical obstacle. Sens. Lett. **14**(1), 26–31 (2016)
19. M. Selmi, F. Echouchene, M.H. Gazzah, H. Belmabrouk, Flow confinement enhancement of heterogeneous immunoassays in microfluidics. IEEE Sens. J. **15**(12), 7321–7328 (2015)
20. R. Abedini-Nassab, M. Pouryosef Miandoab, M. Şaşmaz, Microfluidic synthesis, control, and sensing of magnetic nanoparticles: a review. Micromachines **12**(7), 768 (2021)
21. G.U. Lee, S. Metzger, M. Natesan, C. Yanavich, Y.F. Dufrêne, Implementation of force differentiation in the immunoassay. Anal. Biochem. **287**(2), 261–271 (2000)
22. F. Echouchene, T. Al-Shahrani, H. Belmabrouk, Analysis of temperature-Jump boundary conditions on heat transfer for heterogeneous microfluidic immunosensors. Sensors **21**(10), 3502 (2021)
23. S. Kaziz, I. Ben Mariem, F. Echouchene, M.H. Gazzah, H. Belmabrouk, Design parameters optimization of an electrothermal flow biosensor for the SARS-CoV-2 S protein immunoassay. Indian J. Phys. **96**, 4091–4101 (2022)
24. S. Kaziz, Y. Saad, M. Bouzid, M. Selmi, H. Belmabrouk, Enhancement of COVID-19 detection time by means of electrothermal force. Microfluid. Nanofluid. **25**(10), 1–12 (2021)
25. M. Selmi, R. Khemiri, F. Echouchene, H. Belmabrouk, Enhancement of the analyte mass transport in a microfluidic biosensor by deformation of fluid flow and electrothermal force. J. Manuf. Sci. Eng. **138**(8), 081011 (2016)
26. M. Selmi, R. Khemiri, F. Echouchene, H. Belmabrouk, Electrothermal effect on the immunoassay in a microchannel of a biosensor with asymmetrical interdigitated electrodes. Appl. Therm. Eng. **105**, 77–84 (2016)
27. F. Echouchene, T. Al-Shahrani, H. Belmabrouk, Simulation of the slip velocity effect in an AC electrothermal micropump. Micromachines **11**(9), 825 (2020)
28. F. Echouchene, T. Al-shahrani, H. Belmabrouk, Enhancement of heterogeneous microfluidic immunosensors using new sensing area shape with electrothermal effect. Appl. Sci. **11**(10), 4566 (2021)

29. S. Kaziz, Y. Saad, M.H. Gazzah, H. Belmabrouk, 3D simulation of microfluidic biosensor for SARS-CoV-2 S protein binding kinetics using new reaction surface design. Eur. Phys. J. Plus **137**(2), 1–12 (2022)
30. S. Kaziz, I. Ben Mariem, F. Echouchene, M. Belkhiria, H. Belmabrouk, Taguchi optimization of integrated flow microfluidic biosensor for COVID-19 detection. Eur. Phys. J. Plus **137**(11), 1–12 (2022)
31. F. Shahbazi, M. Jabbari, M.N. Esfahani, A. Keshmiri, A computational simulation platform for designing real-time monitoring systems with application to COVID-19. Biosens. Bioelectron. **171**, 112716 (2021)
32. N. Daneshvar, A. Khataee, M. Rasoulifard, M. Pourhassan, Biodegradation of dye solution containing malachite green: optimization of effective parameters using Taguchi method. J. Hazard. Mater. **143**(1–2), 214–219 (2007)
33. E.Y. Ng, W.K. Ng, Parametric study of the biopotential equation for breast tumour identification using ANOVA and Taguchi method. Med. Biol. Eng. Compu. **44**(1), 131–139 (2006)
34. R. Romero-Villafranca, L. Zúnica, R. Romero-Zúnica, Ds-optimal experimental plans for robust parameter design. J Stat Plan. Inference **137**(4), 1488–1495 (2007)
35. C.-H. Wu, W.-S. Chen, Injection molding and injection compression molding of three-beam grating of DVD pickup lens. Sens. Actuators, A **125**(2), 367–375 (2006)
36. B.J. du Plessis, G. De Villiers, The application of the Taguchi method in the evaluation of mechanical flotation in waste activated sludge thickening. Resour. Conserv. Recycl. **50**(2), 202–210 (2007)
37. J.-Y. Houng, J.-H. Liao, J.-Y. Wu, S.-C. Shen, H.-F. Hsu, Enhancement of asymmetric bioreduction of ethyl 4-chloro acetoacetate by the design of composition of culture medium and reaction conditions. Process Biochem. **42**(1), 1–7 (2007)
38. M. R. Dahman, AMSM-analysis Of variance (ANOVA)-chapter nine. 2018
39. M.A. Sayed, O.M. Dawood, A.H. Elsayed, W.R. Daoush, Application of Taguchi method in optimization of process parameters of ODS tungsten heavy alloys. Adv. Mater. Res. **6**(1), 079 (2017)
40. A. Ramos, H. Morgan, N.G. Green, A. Castellanos, Ac electrokinetics: a review of forces in microelectrode structures. J. Phys. D Appl. Phys. **31**(18), 2338 (1998)
41. M.L. Sin, V. Gau, J.C. Liao, P.K. Wong, Electrothermal fluid manipulation of high-conductivity samples for laboratory automation applications. J. Assoc. Lab. Autom. **15**(6), 426–432 (2010)
42. N.G. Green, A. Ramos, A. Gonzalez, A. Castellanos, H. Morgan, Electrothermally induced fluid flow on microelectrodes. J. Electrostat. **53**(2), 71–87 (2001)
43. M. Zimmermann, E. Delamarche, M. Wolf, P. Hunziker, Modeling and optimization of high-sensitivity, low-volume microfluidic-based surface immunoassays. Biomed. Microdevice **7**(2), 99–110 (2005)
44. K. Li, A. Huang, Q. Huang, *Finite element methods and their applications* (Academic Press, Beijing, 2006)
45. C. Qi et al., Investigation of interaction between two neutralizing monoclonal antibodies and SARS virus using biosensor based on imaging ellipsometry. Biomed. Microdevice **8**(3), 247–253 (2006)
46. K.-R. Huang, J.-S. Chang, Three dimensional simulation on binding efficiency of immunoassay for a biosensor with applying electrothermal effect. Heat Mass Transf. **49**(11), 1647–1658 (2013)
47. C. Naresh, K. Pant, P. Bose, C. Rao, " in *Optimization of Process Parameters on Performance Measures of Wire Electrical Discharge Machining on Niobium C-103 Using Taguchi Method*. Recent Advances in Material Sciences. (Springer, 2019), pp. 409–423
48. A. Lakshminarayanan, V. Balasubramanian, Process parameters optimization for friction stir welding of RDE-40 aluminium alloy using Taguchi technique. Trans. Nonferrous Metals Soc. China **18**(3), 548–554 (2008)